https://doi.org/10.5194/wes-2024-32
Preprint. Discussion started: 17 May 2024

eawe european academy of wind energy
Open Access WIND ENERGY SCIENCE DISCUSSIONS

Periods of constant wind speed: How long do they last in the turbulent atmospheric boundary layer?

Daniela Moreno [1], Jan Friedrich [1], Matthias Wächter [1], Jörg Schwarte [2], and Joachim Peinke [1]

[1]Carl von Ossietzky Universität Oldenburg, School of Mathematics and Science, Institute of Physics. Oldenburg, Germany.
[2]Nordex Energy SE & Co.KG, Erich-Schlesinger-Straße 50, 18059 Rostock, Germany.

Correspondence: Daniela Moreno (aura.daniela.moreno.mora@uni-oldenburg.de)

Abstract. A ~~non investigated~~ feature of the atmospheric turbulent wind, named periods of constant wind speed, is ~~introduced~~ and investigated. We hypothesize that ~~such~~ periods of constant wind speed are related to characteristic wind field structures (e.g., ramps ~~or jets~~), which when interacting with a wind turbine may induce particular dynamical responses. Therefore, this study focuses on the characterization of the constant wind speed periods in terms of their ~~length~~s, probability of occurrence, and extreme events. Atmospheric off-shore wind data are analyzed. Our findings reveal that the statistics of long constant wind speed periods are an intrinsic feature of the atmospheric boundary layer and show the challenging power law behaviour of extreme events, which depends on the local conditions and the precise definition of wind speed thresholds. A comparison to wind time series generated with standard synthetic wind models and to time series from ideal stationary turbulence suggests that these structures are not characteristics of small-scale turbulence but seem to be consequences of larger-scale structures of the atmospheric boundary layer, and thus are a ~~typical~~ multi-scale effect. Given the ~~conclusive~~ results, we show that the Continuous Time Random Walk model, as a non-standard wind model, can be adapted to generate the statistics of those periods of constant wind speed measured from the atmospheric turbulent wind.

1 Introduction

The estimation of the loads experienced by a wind turbine (WT) is fundamental for decision-making processes during the design phase of the various components of the machine, as well as for control strategies during its operation. Such estimation is performed through numerical modelling of the interaction between the WT and the incoming wind. Therefore, an accurate description of the wind within the atmospheric boundary layer (ABL) is essential for correctly calculating the loads acting on the WT. The International Electrotechnical Commission (IEC) (IEC, 2019) has defined the widely-used standard parameters and models for the characterization of the atmospheric wind. These standard wind field models extensively consider the spectral properties and coherence of the velocity components of the wind. Nevertheless, the standard models are designed to mimic the atmospheric wind in a computationally efficient way. As a result, some features of the flow in the ABL are neglected. During the past decades, new challenges in the design process of wind turbines have emerged (Veers et al., 2019). On the one hand, trends in the design of modern WTs account for bigger rotor areas and less rigid structures (i.e. blades) to capture more energy from the available wind resources. On the other hand, the weight and material requirements of each component are

https://doi.org/10.5194/wes-2024-32
Preprint. Discussion started: 17 May 2024

eawe european academy of wind energy
Open Access WIND ENERGY SCIENCE DISCUSSIONS

being pushed to minimal levels. As a result, new WTs are becoming, in general, larger and less rigid. Therefore, some of the characteristics of the atmospheric wind that have been neglected in the IEC standard wind models might become relevant for extra loads not previously considered. Together with the WT manufacturer involved in our research, we concluded that one of these disregarded features is the periods of constant wind speed in atmospheric flows. Such periods are defined as the intervals of time over which the magnitude of the wind speed remains almost constant within a certain range, defined by a threshold value. Such events are important for the functionality of a WT and can lead to beneficial, less noisy working conditions, but also to undesirable increasing dynamics, especially if weakly undamped vibrations are present under such operating conditions. As discussed below, such events are also of general interest for turbulent flows.

The concept of persistence is closely related to our definition of periods of constant wind speed. Persistence characterizes how long a system remains in a particular state before switching to another one. As a general concept, this feature has been investigated in various research fields (Salcedo-Sanz et al., 2022; Grebenkov et al., 2020), such as in economy (Fletcher and Forbes, 2002; Caporale et al., 2022; Nikitopoulos et al., 2022), biology (Arachchige et al., 2021), epidemiology (Kane and T., 2010), and meteorology (Salcedo-Sanz et al., 2021; Lee et al., 2021; Voyant and Notton, 2018). One prominent concept that uses persistence is the so-called zero-crossing method. For a random process $x(t)$ with zero-mean, a zero-crossing corresponds to the waiting time between two successive crossings of its zero. Particularly in turbulence, statistical properties of zero-crossings have been used to characterize quantities like the Taylor micro-scale (Narayanan et al., 1977; Sreenivasan et al., 1983; Kailasnath and Sreenivasan, 1993; Poggi and Katul, 2010) or the integral length scale (Mora and Obligado, 2020; Mazellier and Vassilicos, 2008). Analysis of zero-crossings in atmospheric turbulent data inside canopies, focused on thermal stratification, has been reported (Cava and Katul, 2009; Cava et al., 2012). The scheme of zero-crossings does not investigate the structure of the signal between the crossing, such as possible periods of reduced turbulent amplitudes, in which we are interested. In fact, we introduce a new approach for measuring the events of our study. Nevertheless, the method and statistics of such persistent zero-crossing events are relevant to the discussion. On special interest are self-similar, critical, or fractal features of turbulence that propose a power law behavior for the probability distribution of the time intervals with duration T, which can be formulated as $p(T) \propto T^{-\alpha}$ (in particular for the limit of large T). Such power law statistics may lead to the demanding phenomenon of divergence of mean value or variance, depending on the value of α, and can be taken as proof for scale invariance and extreme events.

From the wind energy perspective, the persistence of the wind is related to the stability and availability of wind resources. These two are essential parameters for the assessment of the power potential, specific details of the design of the WTs, and their control strategies. In this context, correct statistical descriptions of the times over which the magnitude of the wind speed remains at certain conditions are required. Different methods for describing such waiting times have been introduced (Koçak, 2008; Leahy and McKeogh, 2013; Patlakas et al., 2017). However, the available studies using such techniques are mainly focused on characterizing the so-called low-wind-speed events over which very low or no energy is produced. Therefore, the low-wind-speed periods are normally defined for wind speed values below the cut-in thresholds of the WTs. Results on the statistics of low-wind-speed periods have been reported for local data (Ohlendorf and Schill, 2020; Kruyt et al., 2017; Leahy

https://doi.org/10.5194/wes-2024-32
Preprint. Discussion started: 17 May 2024

eawe european academy of wind energy
Open Access WIND ENERGY SCIENCE DISCUSSIONS

and McKeogh, 2013; Patlakas et al., 2017; Sinden, 2007). In common, these studies investigated modeled time series based on extrapolated or reanalyzed local records (Brune et al., 2021).

We characterize the statistics of periods of constant wind speed (with a low level of turbulent fluctuations) from wind measurements in the ABL. In a preliminary investigation (Moreno et al., 2022), the method for the assessment of such events from wind speed time series was presented. First results on the characterization of the periods in terms of their duration and probability distributions were also reported. Special attention within the characterization was given to the tails of the distributions, which describe extremely long periods. Such strong periods are expected to have a stronger influence on a WT. Interestingly, we found that the probability distribution for very long periods shows a power-law decay $p(T) \propto T^{-\alpha}$. Furthermore, a comparison with wind data generated by an IEC standard model (IEC, 2019) revealed that the model underestimates the frequency of occurrence of the extremely long periods measured in the ABL. Along with the mentioned findings, some points remained inconclusive in our initial investigation. These points concern whether these periods are induced by specific orographic perturbations, whether they are laminar or low turbulent structures, and whether they are intrinsic features of a turbulent flow or rather result from large scale interactions within the ABL. As an extension of the work presented in (Moreno et al., 2022), in this study we aim to address such open questions. Firstly, by characterizing the periods of constant wind speed from a different measurement site; and secondly, by comparing the results with experimental ideal turbulent data. Furthermore, a stochastic model is presented as a surrogate wind model to incorporate the statistics of long periods of constant wind speed from turbulence in the ABL.

The paper is structured as follows: Sec. 2 retakes the method for measuring the periods and describes the atmospheric wind data to be analyzed. In Sec. 3, the results of the statistical characterization of the periods from the atmospheric data are shown. In Sec. 4, we compare the results from ABL data to those from two different data sets (i.e. standard and experimental ideal turbulence). In Sec. 5, we present our conclusions and potential future work.

2 Methodology and Data

2.1 Definition of a period of constant wind speed T_c

A period of constant wind speed T_c is defined as the time over which the magnitude of the wind speed $u(t)$ exhibits low-amplitude fluctuations enclosed within certain thresholds (Moreno et al., 2022). A period T_c is depicted in Fig. 1. Over the length of T_c, the wind speed remains inside the *constant speed interval*, $u_{t^*} \pm \varepsilon$, where u_{t^*} is a reference speed value and ε is the maximum acceptable magnitude of the fluctuations around u_{t^*}. In the figure, the horizontal red bars illustrate the thresholds which delineate the constant speed interval. It should be noted that these periods are not laminar, but periods with a smaller amplitude of turbulence; see also Sec. 3.

https://doi.org/10.5194/wes-2024-32
Preprint. Discussion started: 17 May 2024

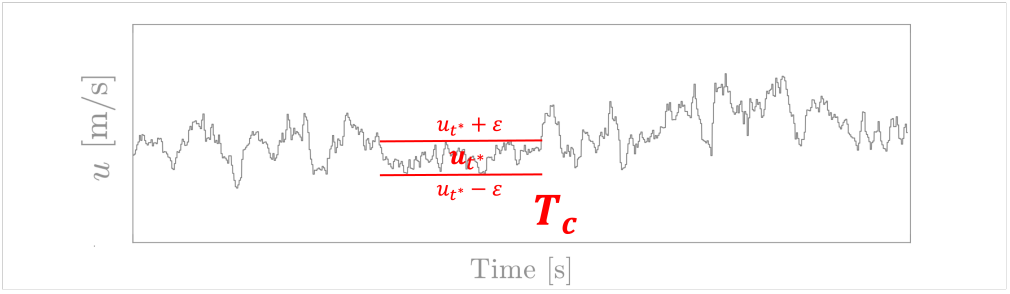

Figure 1. Schematic representation of a period of constant wind speed T_c measured from an exemplary wind speed time series $u(t)$. The *constant speed interval* $u_{t^*} \pm \varepsilon$ specifies the limits for the accepted level of turbulence within T_c.

In the following, the method for measuring the length of a period T_c at a given time step t^* is described. Here we present a more rigorous formulation of the method, compared to the one provided in (Moreno et al., 2022). Essentially, the goal is to count the number N of consecutive time steps, including t^*, for which their wind velocity $u(t)$ is contained inside the constant speed interval. For that, the reference speed $u_{t^*} = u(t^*)$ and the corresponding constant speed interval $u_{t^*} \pm \varepsilon$ is defined. Next, the velocities at the time steps $t^* + i$ for $i = (1, 2, 3..., \infty)$ are evaluated and counted. The counter $\tilde{N}^+$ for the evaluation of $u(t^* + i)$ is then defined as,

$$\tilde{N} = \begin{cases} \tilde{N} + 1 & \text{if } (u_{t^*} - \varepsilon) \leq u(t^* + i) \leq (u_{t^*} + \varepsilon) \\ \tilde{N}; \text{end} & \text{otherwise.} \end{cases} \tag{1}$$

Note that only consecutive points are counted in $\tilde{N}$. The count is concluded once the value of $u(t^* + i)$ exceeds either the bottom or the top limits of the constant speed interval. So far, only points in the forward direction from t^* are evaluated. The same algorithm is subsequently applied to counting the number of points $\tilde{N}^-$ in the backward direction from t^*. In this case, values of $i = (-1, -2, -3..., -\infty)$ are considered for evaluating $u(t^* + i)$ in Eq. (1). Finally, the total number of consecutive points N measured at t^* results from the sum of $\tilde{N}^+$ and $\tilde{N}^-$, independently measured in the forward and backward directions. The length of the period T_c at t^* is then obtained by multiplying the total N by the size of the time step δt.

The method for T_c is performed for every time step in the time series $u(t)$. In the case of overlapping periods, only the longest-measured period is recorded. By doing so, a recounting of events is avoided.

In (Moreno et al., 2022), the threshold ε for fixing the constant speed interval $u_{t^*} \pm \varepsilon$ was randomly selected (e.g. 0.2 - 0.4 m/s). Now, in order to introduce a systematic approach, ε is defined to be proportional to the standard deviation of the wind speed σ_u. Given a wind speed time series $u(t)$, the standard deviation σ_u measures the size of the fluctuations around the mean value $\bar{u}$. Then, ε is calculated as,

$$\varepsilon = A \cdot \sigma_u \tag{2}$$

https://doi.org/10.5194/wes-2024-32
Preprint. Discussion started: 17 May 2024

eawe european academy of wind energy
Open Access WIND ENERGY SCIENCE DISCUSSIONS

where the value of A, typically $A < 1$, can be chosen depending on the particular application. In the case of a WT, A might be related to the thresholds for the control system to operate within different turbulent regimes. In practice, such thresholds in the operating protocols are commonly defined as a function of the turbulence intensity $TI = \sigma_u/\bar{u}$.

2.2 Atmospheric wind data

In (Moreno et al., 2022) data from two different onshore sites were investigated. The onshore wind is strongly influenced by orographic conditions. Therefore, it remained unclear to what extent the the periods T_c were originated by such external conditions. To address this issue, we selected offshore data to be analyzed in this study. We expect such data to provide a better representation of undisturbed, or less disturbed conditions within the ABL compared to onshore data.

Data from the research platform FINO1 (FINO) are investigated. The platform is located in the North Sea and the Baltic Sea. Records of the wind speed were taken by vertically aligned cup anemometers mounted at different heights. The data correspond to a continuous period of approximately five days ($4\text{x}10^5$s), measured in January 2006 with a sampling frequency of 1Hz. Measurements at heights H=[30, 40, 50, 60, 70, 80, 90]m above the mean sea level (MSL) are considered. Fig. 2 shows the mean $\bar{u}$ and standard deviation σ_u calculated over individual 10-minute periods. The complete data set of measurements corresponds to 666 10-minute periods. Exemplary, only the data at H=90m are shown.

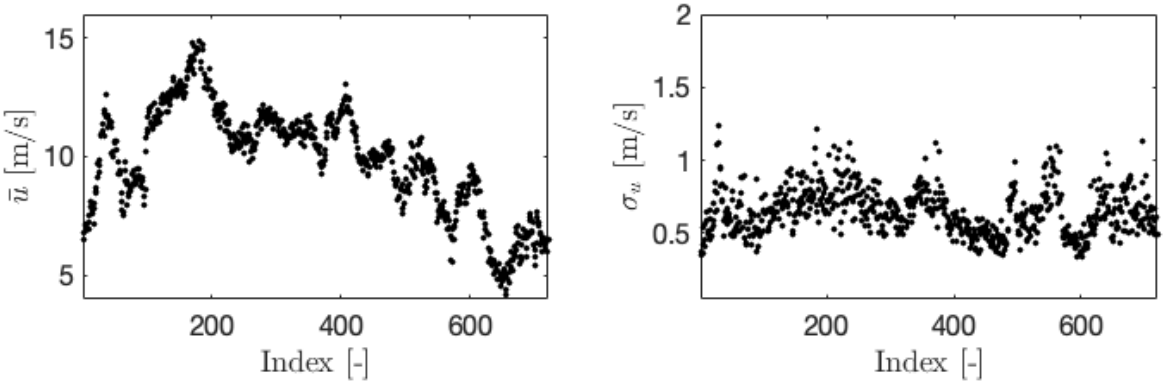

(a) (b)

Figure 2. Wind velocity statistics of FINO data at H=90m over 10-minute intervals (a) Mean wind speed $\bar{u}$. (b) Standard deviation σ_u. Each dot in the plots corresponds to a single 10-min period. The dots are chronologically ordered.

Table 1 summarizes the results for all the heights. There, $\langle\bar{u}\rangle$ and $\langle\sigma_u\rangle$ correspond to the average of the $\bar{u}$ and σ_u over the 666 10-minute intervals at each H. Mean values $\langle\bar{u}\rangle$ vary from 9.7 to 10.0m/s, and the standard deviations $\langle\sigma_u\rangle$ are edged between 0.65 and 0.76m/s.

https://doi.org/10.5194/wes-2024-32
Preprint. Discussion started: 17 May 2024

eawe european academy of wind energy
Open Access WIND ENERGY SCIENCE DISCUSSIONS

H[m]	30	40	50	60	70	80	90
$\langle\bar{u}\rangle$ [m/s]	9.8	9.7	9.8	9.9	10.0	9.9	9.8
$\langle\sigma_u\rangle$ [m/s]	0.74	0.76	0.72	0.71	0.69	0.67	0.65

Table 1. Mean $\langle\bar{u}\rangle$ and standard deviation $\langle\sigma_u\rangle$ of the FINO wind data at the heights H. Angular brackets $\langle\cdot\rangle$ indicate the mean over the 666 subsets of 10 minutes in length.

3 Statistics of T_c for atmospheric turbulent data

3.1 Power spectra of $u(t)$ during periods T_c

The question of whether the wind speed $u(t)$ over the periods T_c is strictly laminar, or rather turbulent with a low degree of turbulence, was outside the scope of our previous work (Moreno et al., 2022). The turbulent nature of $u(t)$ is now verified by the power spectra, shown in Fig. 3. A decay of the form E(f)$\propto$ f$^{-5/3}$ is obtained for all H. Accordingly, the wind data embedded along the periods T_c are not laminar flow sections but periods of turbulence with smaller amplitudes.

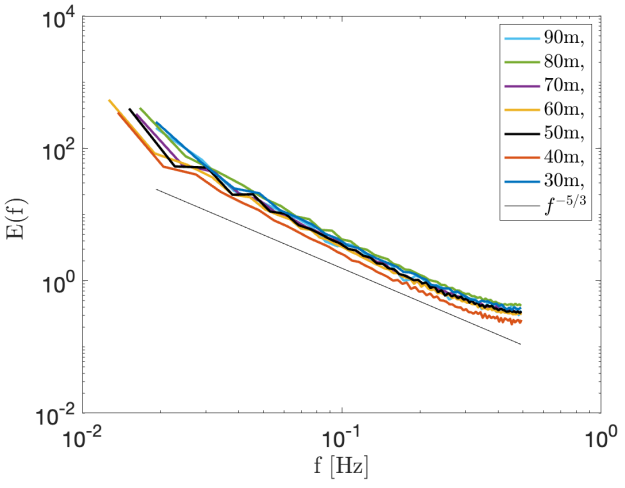

Figure 3. Power spectra E(f) of wind speed $u(t)$ during the measured periods T_c at different heights H. The black solid line shows a decay f $\propto$ f$^{-5/3}$. The spectra are calculated for each period T_c and then averaged over all periods.

3.2 Mean, standard deviation and maximum value of T_c

The statistics of the periods T_c are firstly discussed in terms of the mean duration $\overline{T_c}$, standard deviation σ_{T_c} and maximum value $T_{c,max}$. A factor A=0.3 is exemplary chosen for defining the threshold $\varepsilon = A\cdot\langle\sigma_u\rangle$ for the constant speed interval $u_{t^*}\pm\varepsilon$. With the definitions above, periods with less than 2 % turbulence are selected. The results on the statistics of T_c at different heights H are summarized in Table 2. The values of ε are also provided.

https://doi.org/10.5194/wes-2024-32
Preprint. Discussion started: 17 May 2024

eawe european academy of wind energy
Open Access WIND ENERGY SCIENCE DISCUSSIONS

H [m]	**30**	**40**	**50**	**60**	**70**	**80**	**90**
ε[m/s]	0.22	0.23	0.22	0.21	0.21	0.20	0.20
$\overline{T_c}$ [s]	5.71	5.43	6.14	6.33	6.28	6.47	5.30
σ_{T_c} [s]	5.62	5.32	6.31	6.54	6.44	6.65	4.75
$T_{c,max}$ [s]	104	145	132	158	123	120	91

Table 2. $\overline{T_c}$, σ_{T_c}, and $T_{c,max}$ for different heights H. The values of ε is calculated by considering the value of the standard deviation $\langle\sigma_u\rangle$ at the corresponding H (see Table 1).

Special attention has to be devoted to the meaning of the statistical moments $\overline{T_c}$ and σ_{T_c} calculated from the data. In certain cases, as those presented in (Moreno et al., 2022), the probability distribution $p(T_c)$ may lead to not converging moments, i.e., mean and variance. Further details are discussed next and in Appendix A and Appendix B.

3.3 Probability density function of T_c

Next in the statistical characterization of T_c, the probability density functions (PDF) $p(T_c)$ are discussed. Fig. 4 shows $p(T_c)$ for the corresponding data shown in Table 2 for different H. As mentioned before, we focus our attention on characterizing very long periods T_c as potential sources of special responses of the WTs. Therefore we concentrate on the tails of $p(T_c)$. For comparability, the values of T_c are normalized by the longest measured period at each H; more precisely, we use a representative value $\tilde{T}_{c,max}$ of at least five of the longest periods to become statistically more robust.

The normalized PDFs $p(T_c)$ in Fig. 4 are presented in a log-log scale. In such a representation, a straight line reveals a power-law behavior of the form $p(T_c) \propto T_c^{-\alpha}$ with α as the characteristic exponent. In the figure, such power laws are depicted by solid lines with the same color used for the dots at each H. The corresponding estimated exponents α are given in the legends of the figure. In general, for $\alpha \geq 3$, all the moments of the power-law distribution $p(T_c)$ are defined (see Eq. (B1)). Since this is the case for all values of α in Fig. 4, the moments $\overline{T_c}$ and σ_{T_c} converge for all H. In this way, the results presented in Table 2 provide meaningful information about the characteristics of the periods T_c, regardless of the length of the data. Moreover, since the results for the measurements at all H are enclosed within $\pm 8\%$ of the estimated power-law fitting $\propto T_c^{-\alpha}$, then we conclude that α, or the decay $p(T_c) \propto T_c^{-\alpha}$ is height independent. In addition, the power-law decay is proved to hold for different widths of the constant speed interval. They will be discussed in Sec. 3.4.

The power-law distributions $p(T_c)$ for the offshore data shown in Fig. 4 agree with the obtained for the two onshore sites investigated in (Moreno et al., 2022). Then, the structures T_c are not attributed to a specific terrain or orographic condition. However, as the actual statistics of T_c (i.e. $\overline{T_c}$, σ_{T_c}, $T_{c,max}$, α) vary significantly between data sets, they should be exclusively considered for each location.

https://doi.org/10.5194/wes-2024-32
Preprint. Discussion started: 17 May 2024

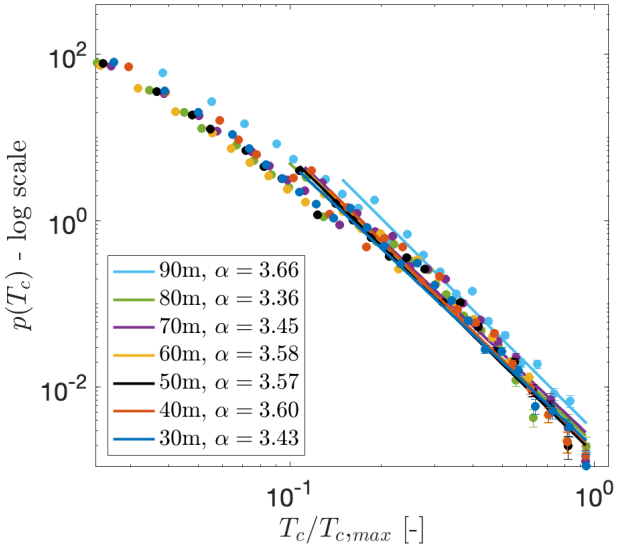

Figure 4. Normalized probability density functions $p(T_c/\tilde{T}_{c,max})$ for FINO data at different heights H. The dots illustrate the results from the FINO data. The solid lines show the power-law decay fitting $\propto T_c^{-\alpha}$. The value $\tilde{T}_{c,max}$ for each height is defined as the bin center containing at least five of the largest measured periods after a binning process.

3.4 Validity of the power-law $\propto T_c^{-\alpha}$

To validate the universality of the power-law behavior, we investigate the effect of the threshold ε by varying the factor A, as $\varepsilon = A \cdot \sigma_u$. Table 3 summarizes the results of $\overline{T_c}$, σ_{T_c}, and $T_{c,max}$ for A=[0.2, 0.3, 0.4, 0.5]. Fig. 5 shows the respective
160 normalized PDFs $p(T_c)$ in an analog representation as shown previously in Fig. 4.

A [-]	**0.2**	**0.3**	**0.4**	**0.5**$(^*)$
ε[m/s]	0.13	0.20	0.26	0.32
$\overline{T_c}$ [s]	3.64	5.30	6.55	12.57
σ_{T_c} [s]	2.33	4.75	6.80	*17.52*
$T_{c,max}$ [s]	45	91	145	392

Table 3. $\overline{T_c}$, σ_{T_c}, and $T_{c,max}$ for different values of the factor A. FINO data measured at H=90m, with $\langle\sigma_u\rangle$=0.65m/s are analyzed. The result of σ_{T_c} for A=0.5$(^*)$ is particularly discussed.

Firstly, Fig. 5 shows a clear power-law decay $\propto T_c^{-\alpha}$ for all values of A. Secondly, we now focus on the case A=0.5, for which results are marked by $(^*)$ in Table 3. As shown in Fig. 5, for this case, a characteristic exponent $2 \leq \alpha \leq 3$ is obtained. Thus, the second moment of $p(T_c) \propto T_c^{-\alpha}$ diverges or is not defined (see Eq. (B1)). In other words, the estimation of the mean of T_c

https://doi.org/10.5194/wes-2024-32
Preprint. Discussion started: 17 May 2024

eawe european academy of wind energy
Open Access WIND ENERGY SCIENCE DISCUSSIONS

leads to $\overline{T_c} \pm \infty$. As a consequence, the estimated value of σ_{T_c} for A=0.5 in Table 3 depends on the length of the time series $u(t)$. This is a prominent feature of distributions with power law tails for which arbitrarily large (with no upper bound) events are expected.

This feature of unbounded periods T_c is also indicated in Table 3. For $A < 0.5$ we see a nearly linear increase of $T_{c,max}$ by about 45s for $A + 0.1$. But for the increase of A from 0.4 to 0.5, the length of $T_{c,max}$ increases more than 200s. For longer time series this value would increase further.

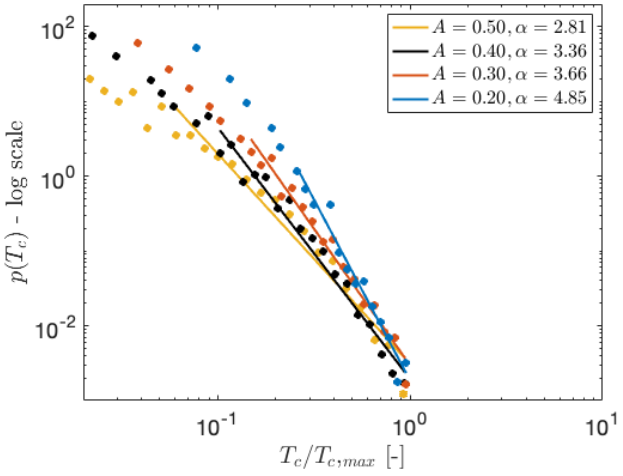

Figure 5. Normalized probability density functions $p(T_c/\tilde{T}_{c,max})$ for FINO data for different values of A. The power-law fittings $\propto T_c^{-\alpha}$ are depicted by the solid lines. Measurements at H=90m, with $\langle\sigma_u\rangle$=0.65m/s are considered. The value $\tilde{T}_{c,max}$ for each value of A is defined as the bin center containing at least five of the largest measured periods after a binning process.

4 Comparison to synthetic wind and pure turbulent data

4.1 Standard-IEC Kaimal and experimental pure turbulence

Another of the open questions in (Moreno et al., 2022) was whether the constant speed periods T_c are typical features of turbulent flow. Therefore, we now investigate the statistics of the periods T_c from experimental ideal turbulent data, namely 'Lab'. This data set was measured by Renner et al. (Renner et al., 2001) in the central region of a free jet, which is approximately stationary, homogeneous, and isotropic. For completeness, we also investigate IEC-standard wind data, labelled as 'Kaimal'. This synthetic data set was generated by the NREL Turbsim package (Jonkman, 2016). Details about the parameters and characteristics of the two additional data sets, 'Lab' and 'Kaimal', are given in Appendix E.

The wind data $u(t)$ from FINO and Kaimal can be compared quite easily as they have comparable characteristics in terms of mean wind speed, standard deviation, sampling frequency, integral length scale, and length of the data. However, fundamental

https://doi.org/10.5194/wes-2024-32
Preprint. Discussion started: 17 May 2024

eawe european academy of wind energy
Open Access WIND ENERGY SCIENCE DISCUSSIONS

differences arise when comparing with the pure turbulent Lab data. To work out the intrinsic features of these different data we used the following three different approaches.

Fig. 6 shows the resulting normalized PDFs $p(T_c)$ for the three wind data sets: (a) FINO, (b) Kaimal, and (c) Lab. The normalization is done by $\tilde{T}_{c,max}$ analogous as in Fig. 4 and Fig. 5. The results in Fig. 6 clearly show different PDFs for the three data sets. The most prominent power-law $\propto T_c^{-\alpha}$ is found for the FINO data. Compared to Kaimal and Lab, FINO data exhibit a slope characterized by smaller values of the characteristic exponent ($\alpha_{FINO} = 3.66$, $\alpha_{Kaimal} = 4.21$, $\alpha_{Lab} = 4.36$). As a result, only the FINO data show a tendency to non-convergence of their lower moments, leading to undefined mean or variance, as well as difficulties in the prediction of extremely large events T_c.

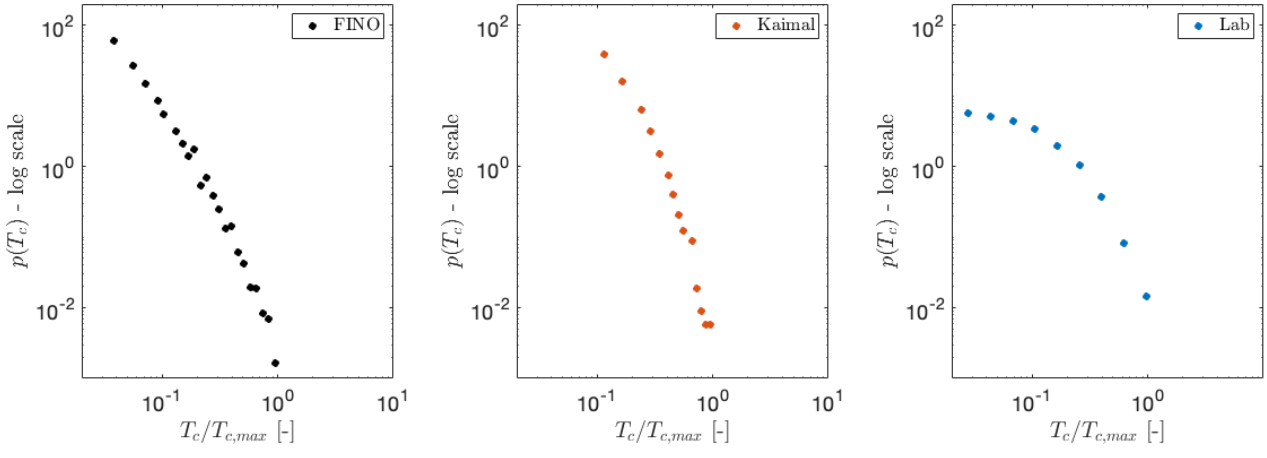

Figure 6. Normalized probability density functions $p(T_c/\tilde{T}_{c,max})$ for (a)FINO, (b)Kaimal and (c)Lab data sets. The value $\tilde{T}_{c,max}$ for each data set is defined after a binning process as the center of a bin containing at least five of the largest measured periods. The constant speed interval is defined with factor A=0.3. Measurements at H=90m are considered for FINO with $\langle\sigma_u\rangle$=0.65m/s. The corresponding σ_u for Kaimal and Lab data sets are 0.58 m/s and 0.38 m/s, respectively.

As a second way to compare the data, we normalize T_c with respect to the total length of the time series L. By doing so, we get information on the absolute duration of periods T_c within the duration of the sample. Results are shown in Fig. 7 (a).

As the results may be affected by the convergence of the data, as a longer data set might introduce different statistics of T_c, we chose a third approach. The integral length scale L_{int} is a measure of the longest correlations, thus we use corresponding PDFs $p(T_c)$ normalized by L_{int}, shown in Fig. 7(b).

https://doi.org/10.5194/wes-2024-32
Preprint. Discussion started: 17 May 2024

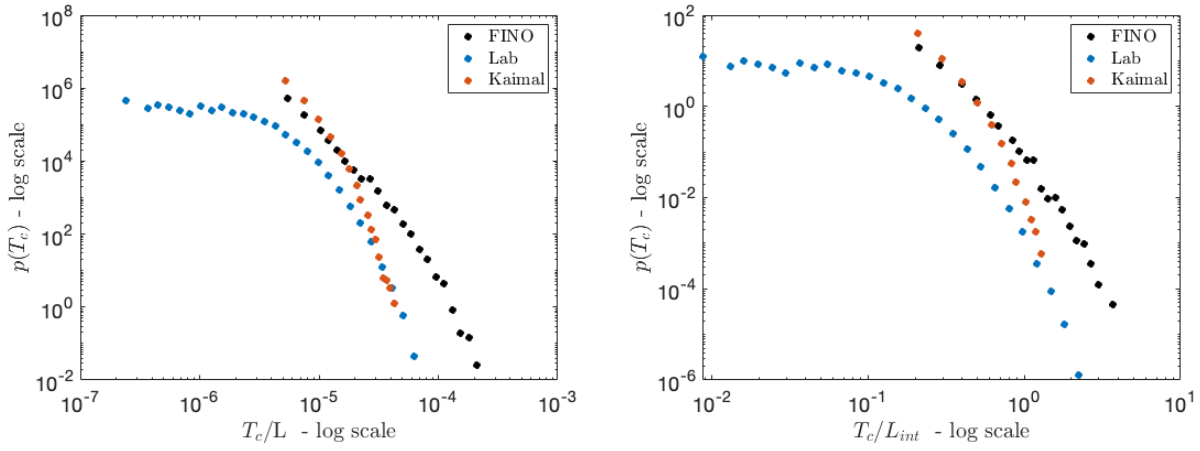

(a) (b)

Figure 7. Normalized probability density functions for FINO, Kaimal and Lab data sets. (a) Normalized $p(T_c/\mathrm{L})$. The value of L is the same for FINO and Kaimal L=4x10^{5}s, and for Lab data L=1062s. (b) Normalized $p(T_c/L_{int})$. The values of L_{int} are 10s and 0.029s for Kaimal and Lab, respectively. The value of L_{int} for FINO is considered to be 10s as a representative value of the atmospheric data.

Comparing the PDFs in Fig. 7, the probability of lower values of T_c/L_x in (a) and (b) for Lab data (blue) is explained by a much higher sampling of the data. The tails of the distributions with the two normalizations, L and L_{int}, show that for the FINO data not only the lengths of periods T_c are larger but also the extremely large events are orders of magnitude more frequent, compared to Kaimal and Lab ($T_c \approx 2L_{int}$ are more than 100 times more frequent for the FINO data than for the other data sets.)

Interestingly, in Fig. 7(b) we note that the three data sets exhibit periods T_c which surpass of the size of L_{int}, or T_c/L_{int}>1. Such structures are large scale structures or may be considered as superstructures (Pandey et al., 2018; Krug et al., 2020). However, for Kaimal and Lab the largest events occur at $T_c \approx 2L_{int}$, while events of length up to $\approx 5L_{int}$ are observed for FINO data.

Furthermore, we calculate the standard deviation of the periods σ_{T_c} in units of integral lengths L_{int}. The resulting values are $\sigma_{T_c,Lab} = 0.12L_{int}$, $\sigma_{T_c,Kaimal} = 0.15L_{int}$, and $\sigma_{T_c,FINO} = 0.47L_{int}$. The estimated values of σ_{T_c} show in another way that FINO data have the tendency of remarkable longer periods, compared to Kaimal and Lab.

4.2 CTRW wind model

We have shown conclusive results on the distributions $p(T_c)$ in the ABL and their underestimation by a standard wind model. Finally, we show how the observed features of the FINO data can be included in a numeric wind field model. As a surrogate for the standard Kaimal model, we investigate non-standard wind velocity time series generated by the Continuous Time Random Walk (CTRW) model (Kleinhans, 2008; Ehrich, 2022; Schwarz et al., 2019; Mücke et al., 2011). The CTRW model generates

https://doi.org/10.5194/wes-2024-32
Preprint. Discussion started: 17 May 2024

eawe european academy of wind energy
Open Access WIND ENERGY SCIENCE DISCUSSIONS

either Gaussian 'CTRW-G' (-G as an abbreviation of Gaussian) or non-Gaussian (-NG as for non-Gaussian wind velocity time series. For the 'CTRW-G', the statistics of $u(t)$ are entirely Gaussian. On the contrary, the statistics of $u(t)$ for the 'CTRW-NG' deviate from Gaussianity towards distributions with so-called heavy tails or higher probabilities of extreme events.

The CTRW model uses a skewed Levy-distributed stochastic process, parameterized by the characteristic exponent α_L, as outlined in more detail in Appendix D and Appendix E. The stochastic process defines a time transformation from the intrinsic scale of the model s to the physical time t. Such time-scaling transformation allows the generation of non-Gaussian time series $u(t)$. The characteristic exponent α_L, with $0 < \alpha_L \leq 1$, specifies the asymptotic behaviour of the skewed Levy distribution. For α_L=1 the resulting process $u(t)$ is entirely Gaussian. Values of $\alpha_L \to 0$ generate processes with more pronounced non-Gaussian characteristics. In this case, non-Gaussianity is related to extremely long waiting times between two successive time steps s. A very long waiting time in $u(s)$ would then be translated into a period over which the process $u(t)$ remains constant.

Fig. 8 shows an excerpt of $u(t)$ for a Gaussian CTRW-G and a non-Gaussian CTRW-NG realizations. Respectively, values of α_L=1 and α_L=0.9 are considered. Along the interval between t=875s and t=895s, a period of almost constant wind speed is observed for the CTRW-NG. For better visualization, a zoomed version of the time series is presented in the sub-figure in the right-bottom corner. Such a structure of the wind, indicated by the horizontal blue line, agrees with our definition of T_c. The observed small fluctuations within the period result from the interpolation process between the intrinsic and the physical times $s \to t$ (Ehrich, 2022).

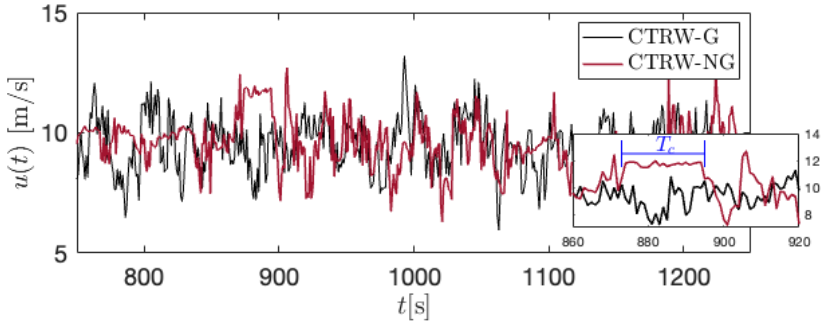

Figure 8. 750-s excerpt of the wind speed time series $u(t)$ for CTRW-G and CTRW-NG. A visible period of almost constant wind speed T_c is visible between 875-895s for the CTRW-NG.

The fundamentals of the CTRW model as well as further details on the method for achieving such non-Gaussian features are given in Appendix D. The parameters for generating the time series are provided in Appendix E.

Fig. 9(a) presents the PDFs $p(T_c)$ for the CTRW realizations, and the FINO data. For FINO, measurements at H=90m are considered. The constant speed interval is fixed with a factor A=0.3. The individual distributions are vertically shifted for better visualization. The dotted lines show the corresponding Gaussian distribution with the mean and standard deviation of the corresponding $p(T_c)$. The grey-shadowed area illustrates the range of the decays of $p(T_c)$ or slopes α, enclosed by CTRW-G

https://doi.org/10.5194/wes-2024-32
Preprint. Discussion started: 17 May 2024

eawe european academy of wind energy
Open Access WIND ENERGY SCIENCE DISCUSSIONS

(□) with α_L=1, and CTRW-NG (△) with α_L=0.9. The distribution of the CTRW-NG realization shows an overestimation, compared to the FINO data, of the deviation from Gaussianity towards a higher probability of very long-duration periods T_c. This deviation is visible from $T_c \approx 0.25/T_{c,max}$. On the contrary, the decay of the CTRW-G is much more pronounced and the divergence from the Gaussian distribution is visible only for events higher than $0.7T_{c,max}$. A third realization, 'CTRW-NG∗', of the CTRW model is compared. This non-Gaussian time series is generated with α_L=0.99. The resulting $p(T_c)$ distribution for CTRW-NG*(○) shows a better agreement with the FINO data. Both distributions, FINO and CTRW-NG*, lie inside the grey shadowed area depicting the slopes enclosed between the Gaussian CTRW-G and extremely non-Gaussian CTRW-NG.

Fig. 9(b) shows the resulting exponents α from the decay $p(T_c) \propto T_c^{-\alpha}$, against the characteristic exponent α_L from the Levy distribution of the CTRW model. The dotted horizontal line depicts the value of α for FINO. We conclude, that by tuning the α_L parameter of the CTRW model, non-Gaussian realizations of $u(t)$ can reproduce the statistics of $p(T_c)$ from the atmospheric turbulent wind.

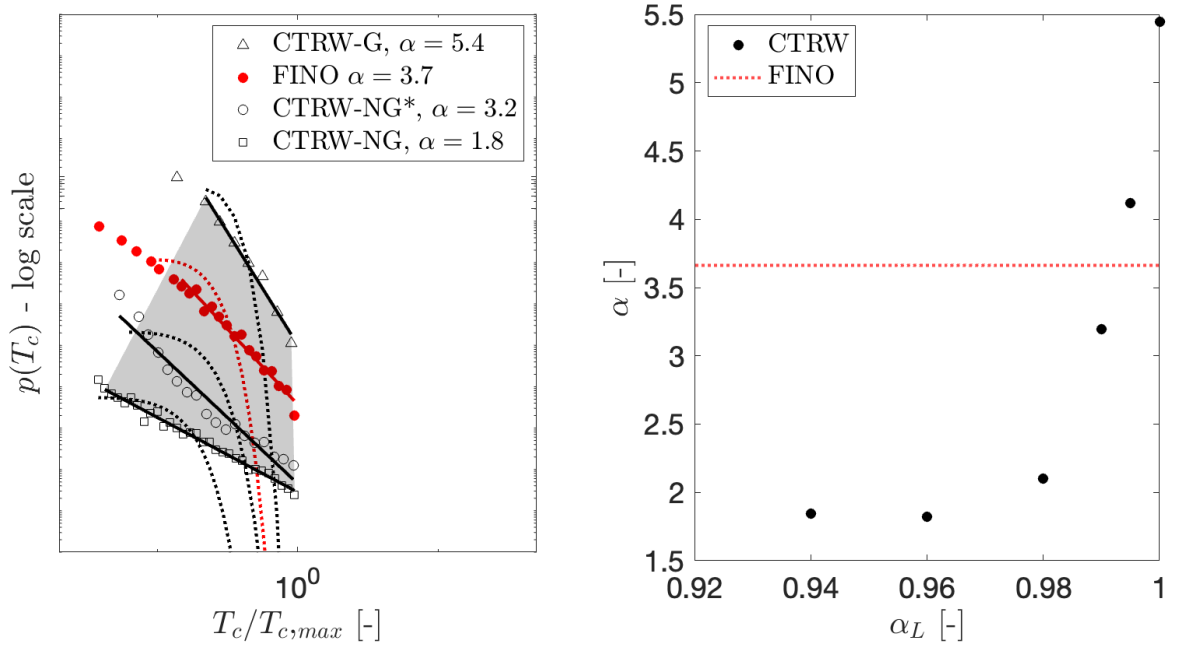

Figure 9. (a) Normalized probability density functions $p(T_c/T_{c,max})$ for the CTRW-G, CTRW-NG, CTRW-NG*, and the FINO data. The individual distributions are shifted vertically for better visualization. Dotted lines depict Gaussian distributions. The grey area depicts the range of the slopes covered between CTRW-G and CTRW-NG. Measurements at H=90m are considered for FINO with $\langle\sigma_u\rangle$=0.65m/s. (b) Power law exponents α from $p(T_c) \propto T_c^{-\alpha}$ as function of the characteristic exponent α_L from the Levy distribution driving the CTRW model.

https://doi.org/10.5194/wes-2024-32
Preprint. Discussion started: 17 May 2024

eawe european academy of wind energy
Open Access WIND ENERGY SCIENCE DISCUSSIONS

5 Conclusions and Outlook

The method introduced in (Moreno et al., 2022) was used to measure the constant wind speed periods T_c (periods with turbulence of a reduced amplitude) from offshore wind data within the ABL. In agreement with (Moreno et al., 2022), we showed that the probability distributions $p(T_c)$ for offshore data also exhibit a power-law decay for very long events. Given that offshore conditions maintain a more unperturbed ABL, we demonstrated that the periods T_c are intrinsic features of the ABL and are not due to specific external agents (i.e. mountains, obstacles). However, significant differences in the values of the critical exponent α presented in (Moreno et al., 2022) suggest that the lengths of T_c are indeed influenced by interactions with the surroundings. Therefore, the estimated statistics of T_c must be considered locally for the specific location of interest. Moreover, from the comparison between different measurement locations of the FINO data, α seems to be quite independent of the height but changes significantly with the threshold ε. Lower values of α are obtained for larger ε. In other words, less pronounced decays of the distribution correspond to wider ranges for considering the wind speed as constant. We found examples of T_c significantly larger than 100s, which correspond to spatially extended structures over sizes larger than 1km, using Taylor's hypothesis of frozen turbulence. Such large structures in a turbulent wind may be related to the so-called superstructures, which are of current interest (Pandey et al., 2018; Krug et al., 2020; Käufer et al., 2023).

We proved the turbulent nature of the wind speed $u(t)$ during the periods T_c. However, the statistics of T_c are significantly different when comparing different turbulent data. Results from experimental pure (ideal) turbulent data suggest that the nature of the periods T_c is attributed to special structures developing in the wind inside the ABL. It is still an open question whether they are caused by special effects of the small-scale turbulence (i.e., different from homogeneous isotropic turbulence) or whether they are indeed consequences of larger-scale interactions of the atmospheric boundary layer, like effects of the spectral gap (Larsén et al., 2016).

We had already shown in (Moreno et al., 2022), that the occurrence of very long T_c events in the ABL is underestimated by the Gaussian assumptions within the standard IEC wind model. Therefore the need for an improved model is justified. The Continuous Time Random Walk (CTRW) model with its newly defined time mapping (see Appendix D) is particularly suitable for the incorporation of the periods T_c measured from the atmospheric turbulent wind. This surrogate model represents an improvement in wind modelling towards more realistic atmospheric wind fields. Consequently, responses of the WT interacting with such disregarded structures on the wind might be better predicted, and critical loads due to these events might be avoided.

From an engineering perspective, constant wind speed periods T_c might be undesirable for the operation of WTs if phenomena such as resonance or critical loading are induced. Still, they also might be profitable if conditions such as constant power production are achieved. In fact, first calculations of the loads induced by periods T_c were investigated by BEM simulations of the 5MW NREL wind turbine (Jonkman et al., 2009). The results suggest that depending on the operational conditions of the WT, certain loads are damped over the period T_c. However, few load sensors, such as the side-to-side bending moment at the base of the tower, are amplified. Therefore, the here presented detailed statistical description of T_c can be useful for control practices. A control system may be adapted to the ε value, as a threshold value when the control dynamics sets in. Our results

https://doi.org/10.5194/wes-2024-32
Preprint. Discussion started: 17 May 2024

eawe european academy of wind energy
Open Access WIND ENERGY SCIENCE DISCUSSIONS

indicate that such a threshold value would lead to fundamentally different T_c statistics, having predictable longest periods or not. On the other hand, some specific aeroelastic events on the WT might be ignored during load simulations for design and control procedures due to inaccurate modelling of such periods within the standard wind models. In special cases, wind field models with improved or extended capabilities to reproduce this feature observed on the atmospheric turbulent wind might become necessary for accurate simulation of the loads and dynamics of the WTs.

A very long period T_c might have an increased impact on a WT depending on its spatial location in the plane of the rotor. The effect of such an event happening in the outer region of the rotor plane might be higher compared to the case when it reaches the turbine at the region near the hub. Within the former scenario, larger moments might be induced on the main shaft or at the root of the blades. Indeed, from the same above-mentioned simulations on the 5MW turbine, the effect on the amplification of the side-to-side moment of the tower increased when considering periods T_c affecting exclusively one quadrant of the rotor plane. Accordingly, in terms of the characterization of such constant wind speeds, future work has to be devoted to evaluating the structures in the spatial domain. Spatial correlations of the periods T_c might be highly relevant for the dynamics of the WT. Afterwards, the complete statistical parametrization of periods of constant wind speeds, in both time and spatial domains, should be assessed and improved for the synthetic wind field models such as the existing CTRW model (Kleinhans, 2008), the recently introduced Time-mapped Mann model (Yassin et al., 2023) which can generate long waiting times of $u(t)$ as in the CTRW model, or the Superstatistical model (Friedrich et al., 2021) that follows the K62 model of turbulence.

Code availability. The algorithm described through Sec. 2.1 for measuring the periods T_c was coded in MATLAB for the analysis of wind speed data. The code can be made available upon request.

Data availability. The FINO and Lab measurements, as well as the generated Kaimal and CTRW time series can be obtained upon request.

Appendix A: Power-law distributions from empirical data

A general quantity x with a probability distribution $p(x)$ follows a so-called *power-law* if,

$$p(x) = C\,x^{-\alpha} \tag{A1}$$

with α as the characteristic exponent and a constant $C = e^c$. The estimation of the exponent α from empirical data has been extensively discussed in the analysis of the distributions of a very wide range of applications (Newman, 2005; Clauset et al., 2009). Since Eq. (A1) is equivalent to $\ln p(x) = -\alpha \ln x + c$, the most simple approach for the calculation of α comes from a linear regression on the log-log plot of the histogram of x. However, this procedure introduces significant errors due to the binning of the data and the resulting distributions. Such distributions are usually dominated by a few bins at lower values of

https://doi.org/10.5194/wes-2024-32
Preprint. Discussion started: 17 May 2024

eawe european academy of wind energy
Open Access WIND ENERGY SCIENCE DISCUSSIONS

x with very high values of $p(x)$, and several bins at the higher range of x with very low probabilities $p(x)$ (Newman, 2005; Dorval, 2008).

Instead of such a linear regression, a logarithmic binning process of the data is recommended. Within this approach, the histogram of x is constructed for k number of bins with variable width. More specifically, the bin edges B are proportional to successive powers of a constant a. Then,

$$B = (b_1, b_2, ..., b_{k+1}) = x_{c,min}(a^0, a^1, ..., a^k) \tag{A2}$$

where $b_1 > 0$, $k > 1$ and x_{min} is the minimum value of x for considering the power-law behaviour. Thus, the i_{th} bin encloses the interval $[b_i, b_{i+1})$ and the larger edge of the k_{th} is assumed to be $+\infty$.

The value of the lower bound x_{min} affects the estimation of the exponent α in $p(x) \propto x^{-\alpha}$. For binned data, b_{min} is defined as the minimum bin taken into consideration for the calculation of α. We follow the algorithm proposed by (Virkar and Clauset, 2014) for choosing b_{min} from binned empirical data. This method is based on a Kolmogorov-Smirnov (KS) statistic test (Massey, 1951) for minimizing the distance between the distributions of the fitted model $P(b|\alpha, b_{min})$ and the empirical model $S(b)$ above b_{min}. Then, the optimized value of b^*_{min} minimizes

$$D = \max_{b \geq b_{min}} |S(b) - P(b|\alpha, b_{min})|. \tag{A3}$$

Further details about the method for calculating b_{min} and α are provided in C.

A distribution with a power-law behaviour is known as critical and may lead to divergent moments. For a quantity x with $p(x) \propto x^{-\alpha}$, the mean value of $p(x)$ becomes infinite for $\alpha \leq 2$. Furthermore, if $\alpha \leq 3$, $p(x)$ has no finite variance (Newman, 2005). In such a case, x can take values of $\bar{x} \pm \infty$ (See Appendix B). Many phenomena, varying from biological to economical, are characterized by critical distributions. A few examples of such variables are the frequency of use of words, the income among individuals, and the magnitude of earthquakes (Newman, 2005; Marquet et al., 2005; Powers, 1998). ~~The latter represents a challenge to the forecasting of seismic events.~~

Appendix B: Statistical moments of power-laws

A power-law distribution of a continuous variable x is defined in Eq. (A1), where $\alpha > 1$ is the power-law exponent and C is a normalization constant. A minimum value x_{min} is defined as the lowest limit at which the power-law holds. Then, the k^{th} moment of a power-law distribution can be calculated.

The k-th moment of the distribution $p(x)$ is given by,

$$\langle x^k \rangle = \int_0^\infty x^k p(x) \mathrm{d}x = \underbrace{\int_0^{x_{min}} x^k p(x) \mathrm{d}x}_{:=A} + \int_{x_{min}}^\infty x^k p(x) \mathrm{d}x = A + \frac{C}{k+1-\alpha} \left[x^{-\alpha+k+1} \right]_{x_{min}}^\infty . \tag{B1}$$

https://doi.org/10.5194/wes-2024-32
Preprint. Discussion started: 17 May 2024

eawe european academy of wind energy
Open Access WIND ENERGY SCIENCE DISCUSSIONS

Then, power-laws with $\alpha \leq 2$ have an infinite mean (k=1). Distributions with $\alpha \leq 3$ have no meaningful variance (k=1). Extensively, the general k^{th} moment exists only if $k < \alpha - 1$.

Appendix C: Estimation of b_{min}

Here we provide the steps we follow for estimating the minimum bin b_{min} above which the power-law $p(T_c) \propto T_c^{-\alpha}$ is valid. The method was proposed by Virkar and Clauset (2014).

For each possible $b_{min} \in (b_1, b_2, ..., b_{k/2})$,

1. Calculate the cumulative binned empirical distribution $S(b)$ for bins $b \geq b_{min}$.
2. Estimate the characteristic exponent $\tilde{\alpha}$ considering $b \geq b_{min}$.
3. Calculate the cumulative density function (CDF) for $P(b|\tilde{\alpha}, b_{min})$ of the binned power-law.
4. Calculate the Kolmogorov-Smirnov(KS) test statistic D defined in Eq. (A3).
5. Select the optimal value b^*_{min} as the value of b_{min} with the minimum test statistic D.

The bins b are defined according to Eq. (A2). For the estimation of $\tilde{\alpha}$ in (ii), a least-squares linear regression method is considered.

Appendix D: CTRW model for the generation of wind fields

More detailed descriptions of the model are provided in (Kleinhans, 2008; Yassin et al., 2023; Mücke et al., 2011; Schwarz et al., 2019). Time series of the wind speed $u_i^{(\kappa)}(t)$ at each point i of a defined grid are based on two coupled Ornstein-Uhlenbeck (OU) stochastic processes $u_r^{\kappa}(s)$ and $u_i^{\kappa}(s)$. Both processes are first generated in an intrinsic scale s. The super index κ accounts for the three directions of the wind $\kappa = [(x), (y), (z)]$. In our case, we generate wind speed time series only in the longitudinal direction $u^{(x)}$, so that $\kappa = (x)$. The two processes are defined as,

$$\frac{\mathrm{d}u_r^{(\kappa)}(s)}{\mathrm{d}s} = -\gamma_r(u_r^{(\kappa)}(s) - u_0^{(\kappa)}) + \sqrt{D_r}\Gamma_r^{(\kappa)}(s) \tag{D1}$$

and,

$$\frac{\mathrm{d}u_i^{(\kappa)}(s)}{\mathrm{d}s} = -\gamma(u_i^{(\kappa)}(s) - u_r^{(\kappa)}(s)) + \sqrt{D_i^{(\kappa)}}\Gamma^{(\kappa)}(s) \tag{D2}$$

where γ and γ_r are damping constants, D and D_r are diffusion constants; and $\Gamma(s)$ and $\Gamma_r(s)$ are Gaussian-distributed white noise. Next, the resulting Gaussian velocity signals $u_i^{(\kappa)}(s)$ are mapped to the physical time scale t by means of an additional stochastic process as,

$$\frac{\mathrm{d}t(s)}{\mathrm{d}s} = \tau_{\tilde{c},\alpha_L}(s). \tag{D3}$$

https://doi.org/10.5194/wes-2024-32
Preprint. Discussion started: 17 May 2024

where $\tau_{\tilde{c},\alpha_L}(s)$ is a Lévy-distributed process with characteristic exponent α_L and a cutoff value $\tilde{c}$. In the case of α_L=1, the intrinsic scales s is equivalent to the physical time t so that $u_i^{(\kappa)}(s)$=$u_i^{(\kappa)}(t)$. The time mapping process described in Eq. (D3) allows the key feature of the model which accounts for the intermittent behaviour of the wind speed time series. The intermittency is introduced by the Lévy-distributed sizes of the waiting times for the transformation from s to t.

In Sec. 4 we investigated two CTRW data sets: CTRW-G and CTRW-NG. The CTRW-G time series were generated with characteristic exponent α_L=1 so that the waiting times of the intrinsic scale s are constant and the statistics of $u(t)$ are Gaussian. For the CTRW-NG time series in Fig. 8 and Fig. 9(a), we assumed α_L=0.9. By doing so, we introduce non-Gaussian features on the probability distributions.

Appendix E: Parameters used for generation of synthetic wind fields

- Kaimal: The data set contains 4 x 10^5 data points with a frequency of 1Hz. The mean wind speed is 10m/s and the standard deviation is 0.58m/s. The integral length scale is set to 10m. The parameters are chosen to be comparable to FINO data (see Sec. 2.2).
- CTRW: Both realizations, 'CTRW-G' and 'CTRW-NG', have 4 x 10^5 data points with a frequency of 1Hz. The mean wind speed and standard deviation are 9.5m/s and 1.1m/s for both cases. Extended parameters for the model are ω_c=1.8Hz; α_L=[0.9 1], $\tilde{c} = 350$ and . Details on the definition of the parameters are given in Appendix D and (Ehrich, 2022). The values of the parameters are chosen to generate data comparable to FINO measurements (see Sec. 2.2).
- Lab: The velocity in the direction of the flow was measured by a hot-wire anemometer. The data set consists of 8.48 x 10^6 points with a sampling frequency of 8kHz. The measured integral length scale is reported as 0.067m (Fuchs et al., 2022). Details of the experiment are found in (Renner et al., 2001).

Author contributions. Daniela Moreno: Development of the code for measuring the periods of constant wind speed from different data sets; generation of the synthetic wind data, analysis of the data and writing the core of the document. Jan Friedrich and Matthias Wächter: Review, analysis, discussion of the results, and contributions to the text. Jörg Schwarte: Discussion on the results from the manufacturer/operator perspective. Joachim Peinke: Extensive understanding of the method, analysis of the results, supervision, reviewing, and editing the text.

Competing interests. The authors declare no conflict of interest. An author is a member of the editorial board of journal WES.

Acknowledgements. We gratefully appreciate the valuable discussions with our partners, the Institute for Mechanical and Industrial Engineering Chemnitz and Nordex Energy SE, involved in PASTA project (Precise design methods of complex coupled vibration systems of

https://doi.org/10.5194/wes-2024-32
Preprint. Discussion started: 17 May 2024

modern wind turbines in turbulent conditions). The aim of this work was initiated as an hypothesis for the challenges discussed within the project.

This work has received funding from the German Federal Ministry for Economic Affairs and Climate Action according to a resolution by the German Federal Parliament (PASTA, 03EE2024).

https://doi.org/10.5194/wes-2024-32
Preprint. Discussion started: 17 May 2024

eawe european academy of wind energy
Open Access WIND ENERGY SCIENCE DISCUSSIONS

References

IEC 61400-1 Wind energy generation systems, Standard, International Electrotechnical Commission, ISBN 978-2-8322-6253-5, 2019.

Arachchige, C., Krishnan, K., Aitken, R., Naidu, R., and Megharaj, M.: Persistence of the parabens in soil and their potential toxicity to earthworms, Environmental Toxicology and Pharmacology, 83, 103 574, https://doi.org/10.1016/j.etap.2020.103574, 2021.

Brune, S., Keller, J. D., and Wahl, S.: Evaluation of wind speed estimates in reanalyses for wind energy applications, Adv. Sci. Res., 18, 115–126, https://doi.org/10.5194/asr-18-115-2021, 2021.

Caporale, G., Gil-Alana, L., and Lasaosa, I.: The impact of the COVID-19 pandemic on persistence in the European stock markets, Heliyon, 8, https://doi.org/10.1016/j.heliyon.2022.e11560, 2022.

Cava, D. and Katul, G.: The Effects of Thermal Stratification on Clustering Properties of Canopy Turbulence, Boundary-Layer Meteorology, 130, 307–325, https://doi.org/10.1007/s10546-008-9342-6, 2009.

Cava, D., Katul, G., Molini, A., and Elefante, C.: The role of surface characteristics on intermittency and zero-crossing properties of atmospheric turbulence, Journal of Geophysical Research: Atmospheres, 117, https://doi.org/10.1029/2011JD016167, 2012.

Clauset, A., Shalizi, C. R., and Newman, M. E. J.: Power-Law Distributions in Empirical Data, SIAM Review, 51, 661–703, 2009.

Dorval, A.: Probability distributions of the logarithm of inter-spike intervals yield accurate entropy estimates from small datasets, J Neurosci Methods, 173, 129–139, https://doi.org/10.1016/j.jneumeth.2008.05.013, 2008.

Ehrich, S.: Analysis of the effect of intermittent wind on wind turbines by means of CFD, Ph.D. thesis, Carl von Ossietzky Universität Oldenburg, 2022.

FINO: FINO1: Forschungsplattformen in Nord- und Ostsee, https://www.fino1.de/en/.

Fletcher, J. and Forbes, D.: An exploration of the persistence of UK unit trust performance, Journal of Empirical Finance, 9, 475–493, https://doi.org/10.1016/S0927-5398(02)00006-3, 2002.

Friedrich, J., Peinke, J., Pumir, A., and Grauer, R.: Explicit construction of joint multipoint statistics in complex systems, J. Phys. Complexity, 2, 045 006, https://doi.org/10.1088/2632-072x/ac2cda, 2021.

Fuchs, A., Kharche, S., Patil, A., Friedrich, J., Wächter, M., and Peinke, J.: An open source package to perform basic and advanced statistical analysis of turbulence data and other complex systems, Physics of Fluids, 34, 101 801, https://doi.org/10.1063/5.0107974, 2022.

Grebenkov, D. S., Holcman, D., and Metzler, R.: Preface: new trends in first-passage methods and applications in the life sciences and engineering, Journal of Physics A: Mathematical and Theoretical, 53, 190 301, https://doi.org/10.1088/1751-8121/ab81d5, publisher: IOP Publishing, 2020.

Jonkman, B.: TurbSim User's Guide V2.00.00, Tech. rep., National Renewable Energy Laboratory, 2016.

Jonkman, J., Butterfield, S., Musial, W., and Scott, G.: Definition of a 5-MW Reference Wind Turbine for Offshore System Development, Tech. rep., National Renewable Energy Laboratory, https://doi.org/10.2172/947422, 2009.

Kailasnath, P. and Sreenivasan, K. R.: Zero crossings of velocity fluctuations in turbulent boundary layers, Physics of Fluids A: Fluid Dynamics, 5, 2879–2885, https://doi.org/10.1063/1.858697, 1993.

Kane, M. and T., G.: Common Threads in Persistent Viral Infections, Journal of Virology, 84, 4116–4123, https://doi.org/10.1128/JVI.01905-09, 2010.

Kleinhans, D.: Stochastische Modellierung komplexer Systeme, Ph.D. thesis, Westfälischen Wilhelms-Universität Münster, 2008.

Koçak, K.: Practical ways of evaluating wind speed persistence, Energy, 33, 65–70, https://doi.org/10.1016/j.energy.2007.07.010, 2008.

Krug, D., Lohse, D., and Stevens, R. J. A. M.: Coherence of temperature and velocity superstructures in turbulent Rayleigh–Bénard flow, Journal of Fluid Mechanics, 887, 2020.

https://doi.org/10.5194/wes-2024-32
Preprint. Discussion started: 17 May 2024

Kruyt, B., Lehning, M., and Kahl, A.: Potential contributions of wind power to a stable and highly renewable Swiss power supply, Applied Energy, 192, 1–11, https://doi.org/10.1016/j.apenergy.2017.01.085, 2017.

Käufer, T., Vieweg, P. P., Schumacher, J., and Cierpka, C.: Thermal boundary condition studies in large aspect ratio Rayleigh–Bénard convection, European Journal of Mechanics / B Fluids, 101, 283–293, 2023.

Larsén, X. G., Larsen, S. E., and Petersen, E. L.: Full-Scale Spectrum of Boundary-Layer Winds, Boundary-Layer Meteorology, 159, 349—-371, https://doi.org/10.1007/s10546-016-0129-x, 2016.

Leahy, P. and McKeogh, E.: Persistence of low wind speed conditions and implications for wind power variability, Wind Energy, 16, 575–575 – 586, https://doi.org/10.1002/we.1509, 2013.

Lee, O., Seo, J., Won, J., Choi, J., and Kim, S.: Future extreme heat wave events using Bayesian heat wave intensity-persistence day-frequency model and their uncertainty, Atmospheric Research, 255, 105 541, https://doi.org/10.1016/j.atmosres.2021.105541, 2021.

Marquet, P., Quiñones, R. A., Abades, S., Labra, F., Tognelli, M., Arim, M., and Rivadeneira, M.: Scaling and power-laws in ecological systems, Journal of Experimental Biology, 208, 1749–1769, https://doi.org/10.1242/jeb.01588, 2005.

Massey, F. J.: The Kolmogorov-Smirnov Test for Goodness of Fit, Journal of the American Statistical Association, 46, 68–78, https://doi.org/10.2307/2280095, 1951.

Mazellier, N. and Vassilicos, J.: The turbulence dissipation constant is not universal because of its universal dependence on large-scale flow topology, Physics of Fluids, 20, 015 101, 2008.

Mora, D. O. and Obligado, M.: Estimating the integral length scale on turbulent flows from the zero crossings of the longitudinal velocity fluctuation, Experiments in Fluids, 61, 199, https://doi.org/10.1007/s00348-020-03033-2, 2020.

Moreno, D., Friedrich, J., Wächter, M., Peinke, J., and Schwarte, J.: How long can constant wind speed periods last in the turbulent atmospheric boundary layer?, Journal of Physics: Conference Series, 2265, 022 036, https://doi.org/10.1088/1742-6596/2265/2/022036, 2022.

Mücke, T., Kleinhans, D., and Peinke, J.: Atmospheric turbulence and its influence on the alternating loads on wind turbines, Wind Energy, 14, 301–316, https://doi.org/10.1002/we.422, 2011.

Narayanan, M. A. B., Rajagopalan, S., and Narasimha, R.: Experiments on the fine structure of turbulence, Journal of Fluid Mechanics, 80, 237–257, https://doi.org/10.1017/S0022112077001657, 1977.

Newman, M.: Power laws, Pareto distributions and Zipf's law, Contemporary Physics, 46, 323–351, https://doi.org/10.1080/00107510500052444, 2005.

Nikitopoulos, C., Thomas, A., and Wang, J.: The economic impact of daily volatility persistence on energy markets, Journal of Commodity Markets, p. 100285, https://doi.org/10.1016/j.jcomm.2022.100285, 2022.

Ohlendorf, N. and Schill, W.-P.: Frequency and duration of low-wind-power events in Germany., Environ. Res. Lett., 15, 1–13, https://doi.org/10.1088/1748-9326/ab91e9, 2020.

Pandey, A., Scheel, J. D., and Schumacher, J.: Turbulent superstructures in Rayleigh-Bénard convection, Nature Communications, 9, 2118, 2018.

Patlakas, P., Galanis, G., Diamantis, D., and Kallos, G.: Low wind speed events: persistence and frequency, Wind Energy, 20, 1033–1047, https://doi.org/10.1002/we.2078, 2017.

Poggi, D. and Katul, G.: Evaluation of the Turbulent Kinetic Energy Dissipation Rate Inside Canopies by Zero- and Level-Crossing Density Methods, Boundary-Layer Meteorology, 136, 219–233, https://doi.org/10.1007/s10546-010-9503-2, 2010.

Powers, D. M. W.: Applications and Explanations of Zipf's Law, in: New Methods in Language Processing and Computational Natural Language Learning, 1998.

https://doi.org/10.5194/wes-2024-32
Preprint. Discussion started: 17 May 2024

Renner, C., Peinke, J., and Friedrich, R.: Experimental indications for Markov properties of small-scale turbulence, Journal of Fluid Mechanics, 433, 383–409, https://doi.org/10.1017/S0022112001003597, 2001.

Salcedo-Sanz, S., Piles, M., Cuadra, L., Casanova-Mateo, C., Caamaño, A., Cerro-Prada, E., and Camps-Valls, G.: Long-term persistence, invariant time scales and on-off intermittency of fog events, Atmospheric Research, 252, 105 456, https://doi.org/10.1016/j.atmosres.2021.105456, 2021.

Salcedo-Sanz, S., Casillas-Pérez, D., Del Ser, J., Casanova-Mateo, C., Cuadra, L., Piles, M., and Camps-Valls, G.: Persistence in complex systems, Persistence in complex systems, 957, 1–73, https://doi.org/10.1016/j.physrep.2022.02.002, 2022.

Schwarz, C. M., Ehrich, S., and Peinke, J.: Wind turbine load dynamics in the context of turbulence intermittency, Wind Energy Science, 4, 581–594, 2019.

Sinden, G.: Characteristics of the UK wind resource: Long-term patterns and relationship to electricity demand, Energy Policy, 35, 112–127, https://doi.org/10.1016/j.enpol.2005.10.003, 2007.

Sreenivasan, K. R., Prabhu, A., and Narasimha, R.: Zero-crossings in turbulent signals, Journal of Fluid Mechanics, 137, 251–272, https://doi.org/10.1017/S0022112083002396, 1983.

Veers, P. et al.: Grand challenges in the science of wind energy, Science, 366, https://doi.org/10.1126/science.aau2027, 2019.

Virkar, Y. and Clauset, A.: POWER-LAW DISTRIBUTIONS IN BINNED EMPIRICAL DATA, The Annals of Applied Statistics, 8, 89–119, 2014.

Voyant, C. and Notton, G.: Solar irradiation nowcasting by stochastic persistence: A new parsimonious, simple and efficient forecasting tool, Renewable and Sustainable Energy Reviews, 92, 343–352, https://doi.org/10.1016/j.rser.2018.04.116, 2018.

Yassin, K., Helms, A., Moreno, D., Kassem, H., Höning, L., and Lukassen, L. J.: Applying a random time mapping to Mann-modeled turbulence for the generation of intermittent wind fields, Wind Energ. Sci., 8, 1133–1152, https://doi.org/10.5194/wes-8-1133-2023, 2023.